Reversible Thermal Gelation in Star Polymers: An Alternative Route to Jamming of Soft Matter

Benoit Loppinet,[†,§] Emmanuel Stiakakis,[†] Dimitris Vlassopoulos,[*,†] George Fytas,[†] and Jacques Roovers[‡]

FO.R.T.H., Institute of Electronic Structure and Laser, Heraklion, Crete, Greece, and NRC, Institute for Chemical Process & Environmental Technology, Ottawa, Ontario, Canada

Received May 7, 2001; Revised Manuscript Received September 5, 2001

ABSTRACT: Crowded solutions of densely branched polymers with starlike architecture undergo a reversible gelation upon heating. This phenomenon is characterized by slow kinetics and is attributed to the formation of clusters causing a partial dynamic arrest of the swollen interpenetrating spheres at high temperatures. A kinetic pseudo-phase diagram of gelation temperature against the effective volume fraction is constructed. Stars with different functionalities exhibit a different sol−gel boundary; small differences in the internal structure of the stars (regular with spherical dense core vs irregular with nonspherical core but spherical overall shape) are presumably responsible for these differences. Thermal gelation is proposed as an alternative route to jamming of soft materials.

I. Introduction

Recently, theoretical and experimental work geared primarily toward the construction of a generic picture of the glass transition and yielding in soft and fragile matter revealed that a wide range of materials such as colloids, emulsions, and foams undergo a jamming transition at low temperatures and/or high volume fractions, which is characterized by a solidlike rheological response.[1,2] The universal features of the jammed systems were represented by a proposed "jamming phase diagram" involving temperature, density, and stress.[1] In the temperature vs density part of this diagram, the conventional behavior of inducing glassy behavior upon cooling and/or increasing density is represented.

Aside from vitrification, a process related to segment-level dynamics (and in any case not a polymer specific property), synthetic polymers can undergo a reversible gelation upon cooling; this is most often due to changes in microstructure (stereochemical reasons), in the absence of other interactions such as electrostatic, enthalpic, or hydrogen bonding.[3] A combination of these factors may drive complex systems such as diblock copolymer micelles to different gel phases or crystals.[4]

However, we showed very recently that the above classification of liquid−solid transitions is by no means complete, in view of the emergence of a novel class of complex materials encompassing both polymeric and colloidal characteristics, tunable at the chemical level, and known as soft (or ultrasoft) polymeric spheres.[5] More specifically, we demonstrated a counterintuitive reversible thermal gelation transition observed in multiarm star polymers and giant block copolymer micelles.[6] These materials were suspended in solvents which are classified as nominally good (but in fact they are of intermediate quality between good and Θ, as discussed below) and characterized by excluded-volume interactions only; upon heating, they exhibited a dramatic increase in their mechanical moduli, eventually yielding a solidlike response. This phenomenon was attributed to the formation of clusters causing a partial dynamic arrest of the swollen interpenetrating spheres at high temperatures, and a kinetic phase diagram was proposed and discussed in analogy to the phase diagram of sterically stabilized colloids; in the latter case colloids crystallized at high volume fractions upon increase of number concentration, whereas the present ultrasoft systems gelled at high volume fractions upon swelling at constant number of stars.

In this paper we examine this novel phenomenon in more detail by considering two types of star polymers ("regular" and "irregular") and addressing in particular two new aspects: (i) the effect of temperature on the conformation of the single star polymers and (ii) the kinetics of the gelation process upon heating and the liquification upon cooling. In the second part we outline the materials and techniques used. Then, in section III we present and discuss the main findings, and finally section IV summarizes the conclusions drawn from this work.

II. Experimental Section

Materials. Using a dendrimer scaffold and chlorosilane coupling chemistry, living linear 1,4-polybutadiene arms were assembled to form regular stars with nominal functionality $f = 128$ and nominal arm molecular weights 28 000, 56 000, and 80 000, coded 12828, 12856, and 12880.[5a] These chemically homogeneous soft materials are called regular stars and are spherical in shape (see illustration in Chart 1a), exhibiting a nonuniform segment density distribution with a higher density toward the core as predicted theoretically and confirmed experimentally.[7−9] Moreover, above the overlap concentration they are characterized by liquidlike ordering due to the enhanced osmotic pressure gradient[9] and by a soft interaction potential.[10] These features are also reflected in their rich dynamic response.[8,11] Further, above a threshold functionality in good solvents there is evidence of a (macro)crystalline phase in a narrow concentration range.[9,12]

A similar chemistry was implemented for the synthesis of 1,4-polybutadiene star polymers of much higher functionality (about 270) and coded LS4 and LS6.[13] In this case, however, a short 1,2-polybutadiene backbone chain was hydrosilylated with $HS(CH_3)Cl_2$, yielding two coupling sites per monomer

[†] Institute of Electronic Structure and Laser.
[‡] Institute for Chemical Process & Environmental Technology.
[§] Present address: University of Sheffield, Department of Physics and Astronomy, Sheffield, U.K.

10.1021/ma010788l CCC: $20.00 © 2001 American Chemical Society
Published on Web 10/04/2001

Chart 1. Schematic Representation of the Structure of a Regular Star (a) and an Irregular Star (b) Polymer; Dashed Circles Attempt To Illustrate the Overall Spherical Shape of These Macromolecular Objects

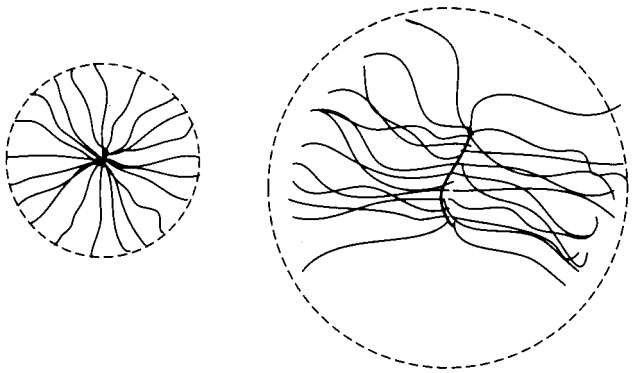

(a) regular star **(b) irregular star**

Table 1. Molecular Characteristics of Regular and Irregular Star Polymers

sample	f	M_a (g/mol)	c^* (mg/mL)[a]	$s = R_h/R_g$[b]
12880	122	72 100	30.6	1.36
12856	127	47 300	45.1	1.32
12828	114	26 100	73.0	1.37
LS4	267	18 300	48.1	1.13
LS6	263	42 300	24.5	1.15

[a] Estimated from the hydrodynamic radius, $c^* = fM_a/[N_A(4/3)\pi R_h^3]$. [b] Data taken from refs 5 and 13 (in cyclohexane) and own measurements.

unit; the latter were substituted with 1,4-polybutadiene by addition of poly(butadienyl)lithium. Because the yield of the hydrosilylation reaction of the polymer did not exceed 80%, the architecture of the resulting highly branched polymer was such that on average four out of five monomer segments are substituted with a total of eight arms. The unsubstituted units are assumed to give some flexibility to the backbone. Because of the absence of a spherical dendritic core, in this case a slightly different internal structure of the star polymer may result, which however apparently retains its overall spherical shape (see also discussion on single stars characterization below). For this reason we call these two polymers "irregular stars" to distinguish them from their regular counterparts (see Chart 1b).

The actual molecular characteristics of the stars studied are summarized in Table 1. The polymers were mixed with decane, a solvent of "intermediate" quality (with a second virial coefficient $A_2 > 0$ which increased with temperature, but not athermal, as discussed below) for 1,4-polybutadiene (see below), followed by gentle stirring at 20 °C for at least 8 h. A small amount (0.1 wt %) of antioxidant (4-methyl-2,6-di-*tert*-butylphenol) was added to eliminate any degradation.

Methods. The dilute solution characterization and the structure and dynamics of concentrated solutions of these dense branched polymers were investigated at different temperatures using shear rheology, small-angle neutron scattering (SANS), and dynamic light scattering (DLS).

A Rheometric Scientific ARES-HR sensitive strain rheometer was utilized with a force rebalance transducer 100FRTN1 in the parallel plate geometry (diameter 25 mm, sample gap about 1 mm). Temperature control in the range of ±0.1 °C was achieved via a recirculating ethylene glycol/water mixture for temperatures between −10 and 70 °C. Measurements included dynamic frequency sweeps and temperature ramps (to determine the gelation temperature), dynamic strain sweeps (to establish the limits of the linear viscoelastic response), and dynamic time sweeps (to quantify the kinetics of the gelation process upon heating and liquification process upon cooling).

Small-angle neutron scattering (SANS) experiments were performed at the ILL D11 spectrometer (sample LS6) in Grenoble. Three distances/collimations were used (20, 5, and 1.5 m) with a neutron wavelength of 6 Å to access the whole scattering wave vector range. Solutions in perdeuterated decane (with 0.1 wt % antioxidant) were measured in 1 mm thick quartz cuvettes and heated to the desired temperatures with an accuracy of ±1 °C.

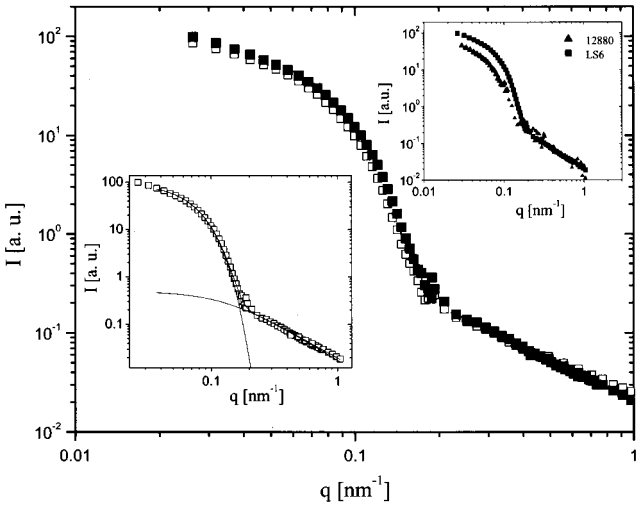

Figure 1. SANS intensities from dilute solution: LS6 0.5 wt % in *d*-decane at 20 °C (■) and 55 °C (□). Lower inset: analysis of the $I(q)$ data of LS6 0.5 wt % using the Dozier fit. The two contributions (form factor at lower q's and blob scattering at higher q's) are clearly visible. Upper inset: comparison between the two stars, LS6 0.5 wt % (20 °C) and 12880 0.1 wt % (47 °C) in *d*-tetradecane. The 12880 intensity has been shifted vertically in order to superimpose the scattering intensities at large q values.

The measurements of the effective hydrodynamic radii of the single polymers (in dilute solution) were carried out with dynamic light scattering by utilizing an ALV goniometer setup and an ADLAS Nd:YAG laser operating at $\lambda = 532$ nm. The Brownian motion of the polymer was detected through the concentration fluctuations of the system at different scattering wavevectors $q = (4\pi n/\lambda)\sin(\theta/2)$, n being the refractive index of the solvent and θ the scattering angle. The time autocorrelation function of the scattered intensity $G(q,t)$ was determined with the aid of an ALV-5000/E fast multi-τ correlator in the time range $10^{-7}-10^3$ s. The measurement consisted of obtaining the intermediate scattering (field) function $C(q,t) = [(G(q,t) - 1)/f^*]^{1/2}$ in the polarized (VV) geometry, where f^* is an instrumental factor relating to the coherence area (for details see ref 11). The equivalent hydrodynamic radius was extracted from the measured diffusion coefficient assuming validity of the Stokes−Einstein relation, $R_h = kT/6\pi\eta D$ (k being the Boltzmann constant and η the solvent viscosity) for spherical objects. The various contributing relaxation mechanisms were detected with measurements of the $C(q,t)$ at high concentrations.

III. Results and Discussion

III.1. Dilute Solution Characterization. *III.1.1. Small-Angle Neutron Scattering.* The dilute solution single star behavior, i.e., the scattering intensity vs q, measured in dilute solution by SANS, is depicted in Figure 1 for two different temperatures and two different stars, a regular 12880 (0.1 wt %) and an irregular LS6 (0.5 wt %); these two solutions are effectively dilute based on the hydrodynamic c^* values of Table 1. It is observed that the data exhibit the typical scattering behavior of multiarm stars,[9b,c] with two apparent distinct contributions at small and large scattering wave vector values. The low-q part is dominated by the "form factor" scattering due to the overall polymer density profile, whereas the high-q part is dominated by the

polymer−solvent fluctuations (blob term). This leads to the representation of the SANS intensity by two independent contributions:[9b,c,14,15]

$$I(q) = P(qR_g) + G(q\xi) \quad (1)$$

where R_g is the radius of gyration and ξ is a correlation length (blob size). Starting from the Daoud Cotton model, Marques et al. recently deduced a rigorous expression for the scattering intensity giving justification for this form.[16] The simplest expression for the form factor is a Guinier type,

$$P(q) = V \exp(-q^2 R_g^2/3) \quad (2)$$

where V is the weight-average molecular volume. The high-q limit $G(q\xi)$ term in eq 1 is approximated by[15]

$$G(q\xi) = \frac{4\pi\alpha}{q\xi} \frac{\sin[\mu \tan^{-1}(q\xi)]}{[1 + q^2\xi^2]^{\mu/2}} \Gamma(\mu) \quad (3)$$

where $\mu = 1/\nu - 1$ (ν the Flory exponent), Γ denotes the gamma function, and α is a normalization constant, treated in this analysis as an adjustable parameter, along with R_g, ξ, and V.

The lower inset of Figure 1 depicts the best fit of eqs 1−3 for the LS6 star at 20 °C, which is indeed very good. Note that the high-q data conform to the $q^{-5/3}$ scaling (eq 3). The obtained values of R_g are known to be underestimated,[9c] primarily because of the insufficient low-q limit (yielding $qR_g \approx 1$, whereas the range $qR_g < 1$ should be reached for an accurate determination of R_g). The R_g values obtained from Figure 1 are 32 nm for 12880 at 47 °C and 25.6 nm for LS6 at 20 °C (26.6 nm at 55 °C). Alternatively, R_g can be obtained from the maximum of a modified Kratky plot ($Iq^{1.67}$ vs q),[9c] yielding respective values of 36 (for 12880), 30.6, and 32 (for LS6) nm. In cyclohexane, a good solvent, the reported values of R_g from light scattering measurements (at 20 °C) are 42.4 nm for 12880[5a] and 55 nm for LS6.[13]

In the upper inset of Figure 1 the comparison between the irregular star LS6 and the regular 12880 is shown.[17] The intensity of the regular star was shifted so that the high-q incoherent intensities superimposed, which is equivalent to a normalization by fN_a^2, with N_a being the arm degree of polymerization; this was necessary given the different solvents, concentrations, and spectrometers used and shows the similarity of the data. Note that the difference in the low-q intensities in the upper inset (normalized to the high-q contribution) conforms to the $f^{3/2}$ scaling.[9c]

Further, from Figure 1 we can note that the swelling due to temperature increase, although directly visible (reduces low-q intensity), remains much less than that observed close to Θ temperature with smaller stars;[14] this is probably due to the fact that in the present work not low enough q's were reached, as already mentioned. On the other hand, this temperature effect provides a justification for the classification of decane as an "intermediate" quality solvent, given the difference from both the Θ and good (athermal) limits.

The suggested molecular shape of the LS molecules based on their synthesis (see Chart 1) implies a possible weak shape anisotropy. However, fitting the form factor $P(q)$ of LS6 using a modified Daoud−Cotton ellipsoid,[18] to account for such an anisotropy, produces virtually identical results with the lower inset of Figure 1, typically for an asymmetry ratio of about 0.85. This suggests that the SANS analysis outlined above is appropriate for the irregular star samples, much like for the regular stars,[9b,c] and further that these experiments cannot probe unambiguously a small deviation from spherical shape. In addition, dynamic depolarized light scattering measurements from dilute LS6 solutions in decane (0.008 wt %) did not reveal any anisotropy. (Some anisotropic scattering was detected at higher concentrations, but this was probably due to second-order scattering effects.[17]) Thus, for all practical purposes here the irregular LS polymers are considered as having a virtually spherical overall shape. Yet, internally their structure differs from that of the regular stars, as outlined in the synthesis part, as the core of the latter is spherical and dense. In fact, from dilute solution measurements in good solvent cyclohexane,[5,13,19] it is apparent that the irregular LS stars exhibit a small deviation from the Daoud−Cotton scaling[7a] $R_g \sim f^{1/5}N^{3/5}$: the ratio of R_g to $f^{1/5}N^{3/5}$ for stars of varying arm molecular weight was about 0.25 for functionalities $f =$ 4−128 and 0.29 for $f = 270$. Such a difference seems also reflected in the dilute solutions measurements which provided the static (R_g) and hydrodynamic (R_h) radii. As seen in Table 1, the ratio $s = R_h/R_g$ for the same solvent (toluene) was found to be about 1.35 for the regular stars and 1.15 for the irregular stars. Actually, values of "s" below the hard-sphere limit (actually this is a constant density sphere) of 1.29 are usually attributed to deviations from sphericity or to lower density in the core region in the irregular compared to the regular stars,[20] a reasonable possibility on the grounds of the representation in Chart 1 and the above discussion. However, such an effect is rather small as it was not clearly resolved in the SANS measurements. Furthermore, it should be noted that the shape of the single macromolecules does not seem to change upon heating, as evidenced from the SANS data (Figure 1).

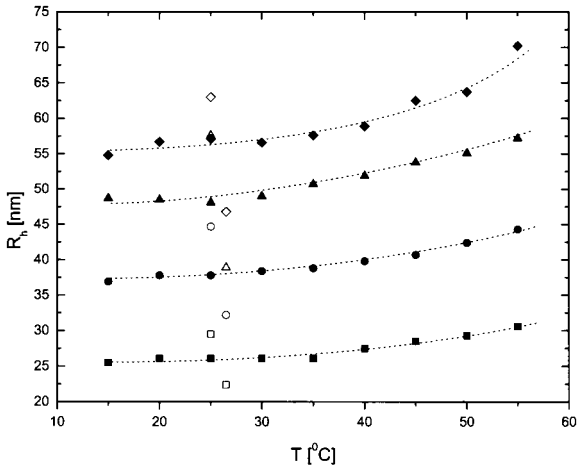

Figure 2. Temperature dependence of the effective hydrodynamic radius of the regular stars 12880 (▲), 12856 (●), and 12828 (■) and the irregular star LS6 (◆), as obtained from dynamic light scattering measurements in dilute solutions ($c < c^*$). The lines are drawn to guide the eye. Respective open symbols refer to the values in a good solvent cyclohexane at 25 °C (high values) and a Θ solvent dioxane at 26.5 °C (low values).

III.1.2. Light Scattering. The effect of temperature is important in influencing the size and is clearly shown in Figure 2, where the temperature dependence of the

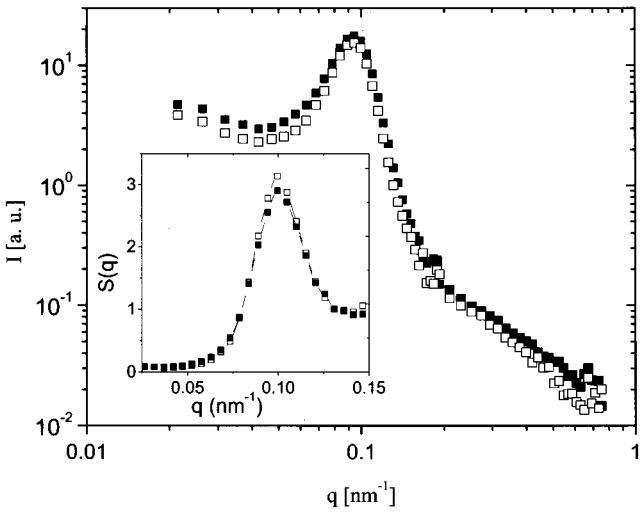

Figure 3. SANS total scattering intensity from 5.4 wt % solutions of LS6 in *d*-decane, at 20 °C (■) and 55 °C (□). Inset: the corresponding extracted effective structure factors $S(q)$, as discussed in the text.

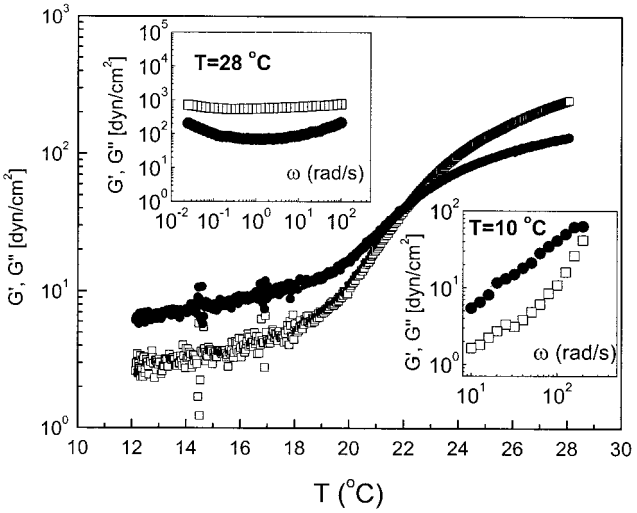

Figure 4. Dynamic temperature ramp of a LS6/decane 5 wt % solution, at a frequency of 5 rad/s and with a heating rate of 1 °C/min, indicating the thermal liquid−solid transition (G', □; G'', ●). Lower inset: dynamic frequency sweep of the same sample at a temperature of 10 °C, in the liquid regime. Upper inset: respective dynamic frequency sweep at a temperature of 28 °C, in the solid regime.

effective hydrodynamic radius of various regular and irregular star polymers is plotted; in all cases concentrations $c < c^*$ from Table 1 were measured. The significant swelling upon heating (about 15%) further suggests that decane is not a truly good (athermal) solvent near room temperature and only approaches good solvent behavior above 55 °C; in fact, the open symbols around room temperature in Figure 2 indicate the limiting R_h values for dioxane (at 26.5 °C, lower value) and cyclohexane (at 25 °C, upper value). The former is a Θ solvent for 1,4-polybutadiene ($\theta = 26.5$ °C) whereas the latter is a good solvent. Therefore, decane is a solvent of intermediate quality, exhibiting a strong temperature dependence in the range investigated. Below we shall use R_h as an index of star dimension. This is of course a dynamic length, but on the other hand, for high functionality stars the hydrodynamic solvent draining is not expected to be severe,[5,19] and thus it should not be influenced by temperature or concentration, so the observed effects relate indeed to star size changes.

III.2. Behavior in Dense Solutions. *III.2.1. Structural Features.* Above the overlap concentration, the star−star interactions give rise to a strong maximum in the scattered intensity. The expression for the intensity is then given by[16]

$$I(q) = P(q)\, S(q) + G(q) \qquad (4)$$

where $S(q)$ is the star's structure factor. Note that both $P(q)$ and $G(q)$ depend on concentration,[9c,16] rendering direct access of $S(q)$ difficult. However, in our case the stars that are typically in the concentration range $c^* < c < 20c^*$ are only slightly interpenetrating, as evidenced by the little variation of the crossover between the form factor low-q regime and the blob high-q regime (Figures 1 and 3), the cooperative diffusion speed-up,[6,11] and the rather small variation of R_g in this range.[9c] We extract $S(q)$ at different temperatures (see inset of Figure 3) by assuming no change in the form factor. This procedure includes subtracting the blob "incoherent" part of the scattering at high q's ($I_i(q) - G_i(q)$), as determined by fitting (eq 3), and then dividing to the star−star contribution ($I_c(q) - G_c(q)$), yielding an effective structure factor:

$$S(q) = (I_c(q) - G_c(q))/(I_i(q) - G_i(q)) \qquad (5)$$

We observe a very small variation in $S(q)$ with temperature. Given the approximations used in this procedure, it is reasonable to state that there is no measurable difference in $S(q)$ with temperature, both in the position of the structural maximum, q_{peak}, and in the intensity. From the inset of Figure 3 it is possible to obtain an estimate of the typical length scale $d \approx 2\pi/q_{peak}$ which is 66 nm, with $R_{h,20} < d < 2R_{h,20}$ ($R_{h,20}$ being the hydrodynamic radius at room temperature); this finding suggests star interpenetration and possibly squeezing in the crowded solutions. In addition, the fact that this distance d does not change with temperature may suggest the interplay of swelling and interpenetration at higher concentrations. Note that the measurements at high temperatures were taken after the sample was equilibrated for more than 1 h at the specific temperature (see also discussion in reference to Figures 7 and 8 below).

III.2.2. Linear Rheology. The effect of temperature in inducing a liquid−solid transition is characteristically depicted in the rheological data of Figure 4 for a LS6 5 wt % solution. The dynamic temperature ramp at a frequency of 5 rad/s, strain 0.5%, and a low heating rate 1 °C /min identifies this transition at 21 °C. A confirmation comes from the frequency spectra, which show that at lower temperatures the polymer solution remains liquidlike (lower inset), and at higher temperature it has a solidlike response (upper inset). It is clear that as the temperature increases, the material behavior changes drastically from viscous liquid (terminal behavior with $G' \sim \omega^2$, $G'' \sim \omega$, $G'' > G'$) to a weak elastic solid (terminal behavior with $G' > G''$ and a very weak frequency dependence), accompanied by an increase in the values of the moduli by 2 orders of magnitude. The reproducibility of these results at different times following cooling to room temperature and recovering the original liquid confirms the reversibility of the process

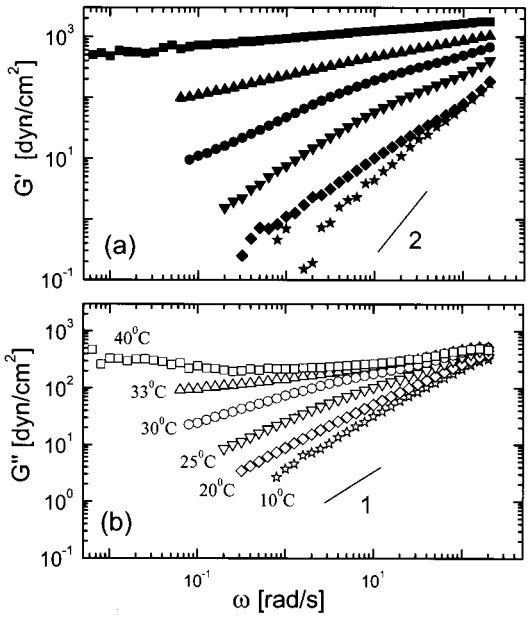

Figure 5. Dynamic frequency sweeps of G' (a; closed symbols) and G'' (b; open symbols) for 12856 5 wt % in *n*-decane at different temperatures across the gelation transition (★, 10 °C; ◆, 20 °C; ▼, 25 °C; ●, 30 °C; ▲, 33 °C; ■, 40 °C).

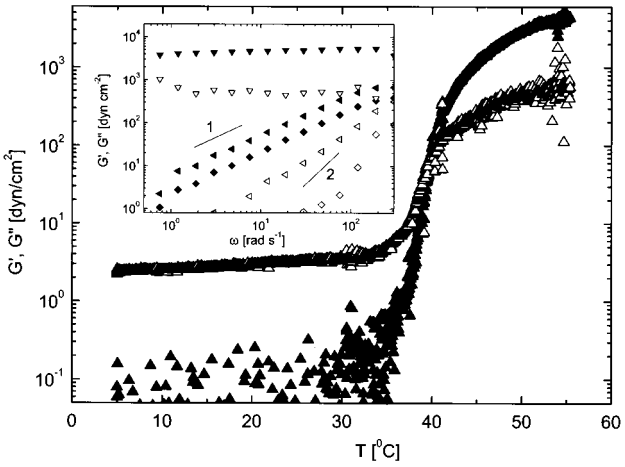

Figure 6. Determination of the gelation temperature for a 12828 8.5 wt % in *n*-decane from the combination of dynamic temperature ramps (5 rad/s, 0.1 °C/min; G', ▲; G'', △) and dynamic frequency sweeps in the inset (▼, 55 °C; tilted ▲, 20 °C; ◆, 5 °C; G', closed symbols; G'', open symbols).

and is consistent with visual observations of this transition. In fact, other star samples exhibiting a liquid−solid transition below room temperature remained immobile at that temperature over the course of a few days, whereas they flowed after being stored in the deep freezer (about −10 °C) for several hours. It is interesting to note that the opposite effect is observed in low functionality star ($f < 32$) and linear polymers, which exhibit the typical Arrhenius temperature dependence (moduli decreasing with temperature); in these cases swelling is insufficient to maintain or enhance η_0.

Figure 5 depicts a systematic evolution of the linear viscoelastic spectra of 12856 with increasing temperature, from the liquid regime to the solid regime. Note that these are equilibrium measurements, meaning that before each measurement (at a certain temperature) enough time had elapsed in order to ensure (using dynamic time sweeps) that the data had become time-independent (see also relevant discussion in connection with Figures 7 and 8 below). It is interesting that there is a distinct change of the frequency dependence of the moduli G' and G'' with temperature, which sometimes can be sharper. This suggests that the swelling of the star (see also Figure 2) enhances the "crowding" of the suspension and is accompanied by some further interpenetration[6] and possible deformation, resulting in a different rheological behavior. In fact, the frequency dependence of G' and G'' over the experimental window (about 3 decades) is indicative of the nature of the formed solid. From the rheological data and additional evidence from scattering and self-diffusion data (see also ref 6 and discussion in conjunction with Figure 3), the solid is identified with a gel. In fact, it is known that if a self-similar gel is formed as discussed in the theory of percolation, then $G' \sim G'' \sim \omega^n$, where the exponent n takes values in the range 0.2−0.5 and relates to the gel's fractal dimension.[21] On the other hand, percolation may not hold for the noncritical gels, as already demonstrated in a variety of gelling soft systems, and most notably concentrated solutions of block copolymer micelles, which have many common features to the stars.[22] Therefore, heating the stars does not necessarily lead to formation of critical gels.

The features of the rheological response across the gelation transition are the same in the regular and irregular star polymers, as seen from the comparison of the temperature ramps and frequency sweeps (Figure 6 for 12828 8.5 wt % and Figure 4 for LS6 5 wt %). The difference in moduli values in these two examples relates to different concentrations and different heating rates used. A rough estimation of the gel time for a given temperature jump from the liquid into the gel region, t_{gel} (from the approximate tan $\delta \sim \omega^0$ criterion[21] or simple time sweeps after the temperature jump), suggests that t_{gel} decreases with increasing temperature.

III.2.3. Kinetics of the Liquid−Solid Transition. An important consideration relates to the kinetics of gelation upon heating and the subsequent liquification upon cooling. This is relevant as the experimental gelation temperatures T_{gel} should be determined close to pseudo-equilibrium (as the gel is actually a nonequilibrium state from the thermodynamic point of view). Figure 7 demonstrates that this pseudo-equilibration time for obtaining a heating-induced gel is rather long; this depends of course on the measurement temperature for a given concentration. It can be seen that it takes considerable time to reach a steady-state response ("equilibrium") in the heating-induced gels; this is very important as it is possible to start a measurement at a certain temperature where the system originally behaves as a liquid, and then over time it solidifies at that temperature (Figure 7a). Typical results from kinetic experiments when cooling the gels are presented in Figure 7b, where the moduli decrease substantially with time at a constant temperature ($G' > G''$ at short times), and eventually the liquid dense star suspension is recovered; note that the scattering of the data at long times is due to the limits of torque resolution in the rheometer (moduli are very small).

Additional support comes from dynamic light scattering measurements. Figure 8 depicts the intermediate scattering function for a 5.5 wt % 12856 solution in decane at $q = 0.033$ nm^{-1}. At high temperature (55 °C) this solution gels, and $C(q,t)$ is characterized by a three-step decay; starting from short times, the relaxation modes are identified[6,11] with the cooperative diffusion

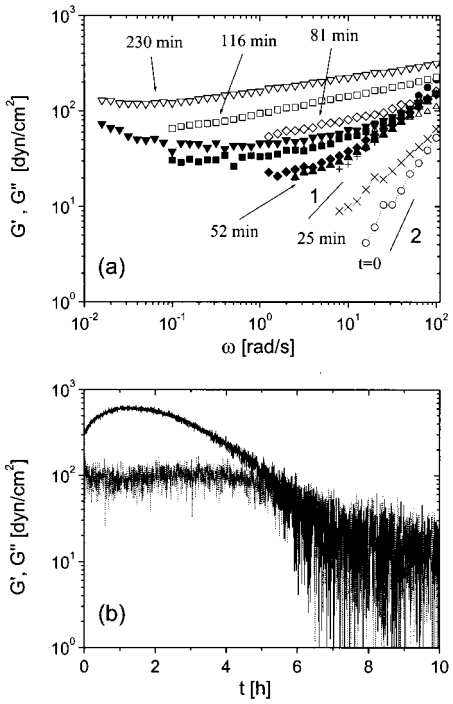

Figure 7. (a) Linear viscoelastic spectra (G', G'') of regular star 12880 5.2 wt % in *n*-decane at 7 °C (taken through a jump from about −10 °C) and different times, demonstrating the long gelation kinetics (○, ●: original measurement at time $t = 0$ after the temperature was reached; ×, +: $t = 25$ min; ▲, △: $t = 52$ min; ◆, ◇: $t = 81$ min; □, ■: $t = 116$ min; ▽, ▼: $t = 230$ min). (b) Representative dynamic time sweeps upon quenching 12880 3.9% in decane to 20 °C (from 45 °C) at 1 rad/s, showing the long time for liquefaction.

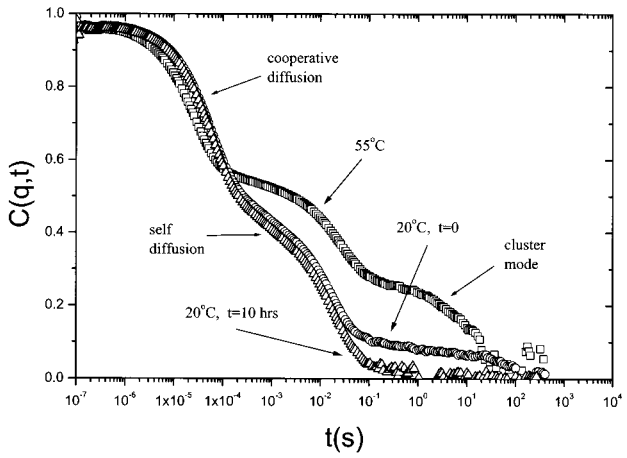

Figure 8. Normalized intermediate scattering function of a 5.5 wt % 12856 star solution in decane at a value of the scattering wavevector $q = 0.033$ nm^{-1}, measured at 55 °C in the gel state and at different times upon subsequent cooling to 20 °C in the liquid state. The various relaxation processes are indicated by arrows. Note that the gel state is characterized by the slow cluster mode which loses intensity upon cooling and eventually disappears when the equilibrium liquid is recovered (after 10 h).

(due to interpenetrating arms), the self-diffusion of stars (colloidal nature), and the slow cluster mode which relates to the gel. Upon cooling to 20 °C which corresponds to the liquid state, the cluster mode loses intensity, and after 10 h it disappears and the equilibrium liquid semidilute star solution is recovered. Therefore, the cluster mode is an identifying signature of the gel; note also that the equilibration time conforms to the rheological experiments (Figure 7b).

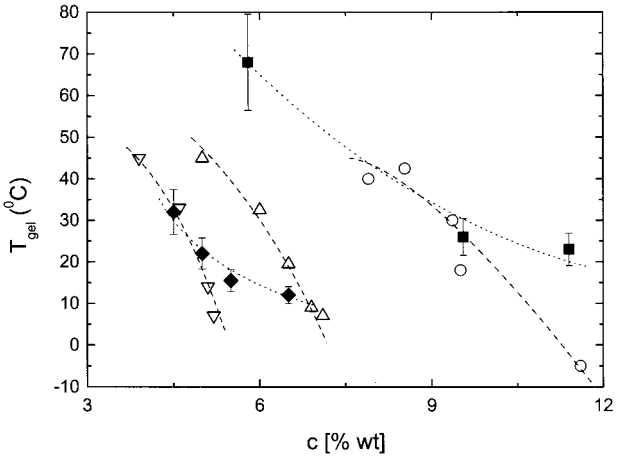

Figure 9. Gelation temperature, T_{gel}, as a function of polymer concentration, *c*, for the stars investigated: 12880 (▽), 12856 (△), 12828 (○), LS4 (■), and LS6 (◆). Lines are drawn to guide the eye.

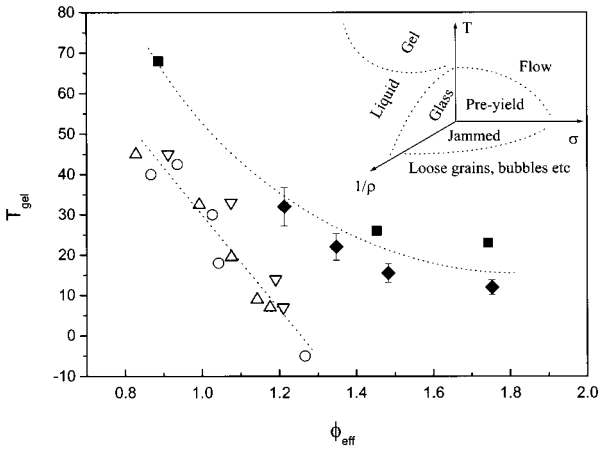

Figure 10. Proposed generalized jamming phase diagram for regular and irregular star polymers. Lines are drawn to guide the eye. Symbols are the same as in Figure 9. Inset: generalized jamming phase diagram proposed by Liu and Nagel[1] in terms of temperature *T*, inverse density (or concentration) $1/\rho$, and stress σ, indicating the speculative interface separating flowing from not-flowing soft materials. In the temperature-inverse density plot the liquid−gel diagram represents the alternative route to jamming proposed in this work.

III.2.4. Toward a Kinetic Phase Diagram. With the "equilibrium" gelation temperatures being determined from the combination of temperature ramp tests, time sweeps, and frequency sweeps, it is now possible to proceed with mapping the results into a kinetic pseudo-phase diagram. Figure 9 plots the T_{gel}'s of the various star polymers as a function of concentration. For all systems it is observed that T_{gel} decreases with increasing concentration. It should be emphasized that for regular stars of functionality $f = 64$ no gelation was detected; concentrated solutions in decane exhibited an enhancement of moduli with temperature (up to 80 °C) but did not gel. Thus, functionality, which primarily affects the core size,[7] plays an important role in the gelation process.

Figure 10 depicts an attempt to obtain a "universal jamming phase diagram" for all stars investigated in this work. The gel temperature T_{gel} is plotted against the effective volume fraction ϕ_{eff} which is essentially the volume fraction of the spherical stars by considering their overall dimension as if they were hard spheres; it is estimated from the weight concentration and their

radius R_h (in the low-temperature liquid region of Figure 2). Note that even for the LS samples we used the same reduction in concentration. The fact that ϕ_{eff} exceeds unity is due to mutual arm interpenetration. The virtual collapse of the T_{gel} data for the different regular stars (all with the same nominal functionality $f = 128$) is an interesting result. However, the irregular stars appear to behave differently and form another sol−gel boundary. Given the similar overall shape of these two types of stars (probed within the resolution of the experimental techniques available), their only difference relates to their internal structure. As already mentioned, the regular stars have a spherical core with virtually constant and high monomer density, whereas the irregular ones have a rather nonspherical core with lower density and a different (nearly double) functionality. Hence, the plot of T_{gel} against ϕ_{eff} does not collapse all data, pointing to the need for an appropriate scaling to accomplish this; but this task is left for future studies as it requires further experimental work and thorough understanding of the phenomenon.

III.2.5. Assessment of the Liquid−Solid Transition: Glasslike Gelation. The phenomenological evidence presented above provides the necessary ingredients for the formation of gels on heating: dense star solutions (above c^*); high functionality (above a threshold value of about 64); solvents of intermediate quality. These conditions hold the key for the consideration of possible mechanisms of this phenomenon. Note also the reversibility of the process excludes the possibility of chemical cross-linking or solidification due to solvent evaporation.

A first issue of substance here is the structural characterization of the heating-induced solid and its difference from the viscous liquid at lower temperartures. This was addressed with the SANS investigation of the regular and irregular star polymers across the gelation temperature as discussed with respect to LS6 and Figure 3. In this figure, the low and high temperatures correspond to the liquid and solid regions, respectively. The results are in good qualitative agreement with the respective information from regular stars 12856 (6 wt % in *d*-decane) as discussed in ref 6. Therefore, as the structural changes upon heating of all stars are found to be insignificant, it is then evident that the observed solidification is not due to any strong structural rearrangements (for example, leading to crystallization[9a]). In addition, the observed phenomenon with the long transients and hysteresis upon heating to gel and cooling to liquid (Figure 7) also suggest analogies to first-order transitions; to elucidate this point, we carried out DSC measurements at typical heating rates of 20 °C/min, and no evidence of latent heat was observed. This situation is also reminiscent of phase separation kinetics relating to the occurrence of a lower critical solution temperature (LCST) demixing;[23,24] however, this possibility is excluded as well, as there was no visual or structural evidence of such transition. (SANS and dynamic light scattering experiments did not show any increase of the scattered intensity across T_{gel},[6] as would have been expected in the case of demixing.) Furthermore, measurements with linear and star polymers in different hydrocarbons (tetradecane) did not reveal any evidence of demixing, based on the same quantitative criteria.[25]

Also, the hysteresis effects suggest analogies with the aging observed in glassy systems[26,27] and seem associated with the temperature-induced swelling,[6] as also

Chart 2. Sketch of the Proposed Thermal Gelation Transition; upon Heating, Single Stars Swell (a) and Dense Star Solutions "Jam" and Form Random Clusters (b)

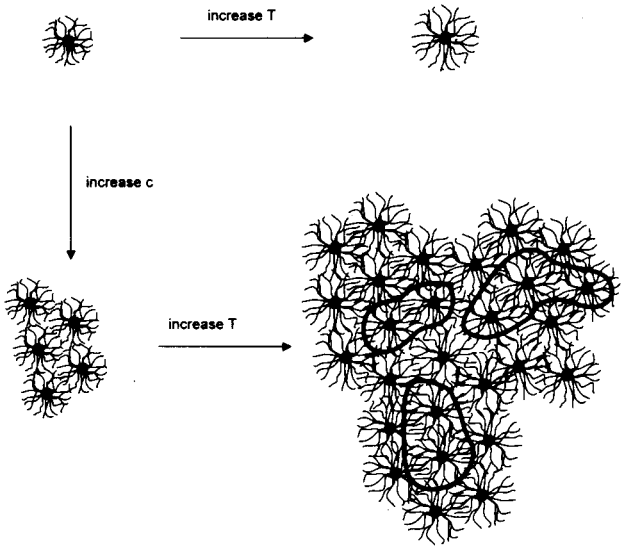

discussed below. Hence, the observed phenomenon is of dynamic origin. From the above discussion, however, there is a likelihood of relating this thermal liquid−solid transition to some type of colloidal glass transition; we believe that this should be ruled out on the grounds of dynamic light scattering measurements which did not reveal any evidence of α-relaxation or related processes.[6,26−28] In addition, it is noted that the gels formed are rather weak, as inferred from the low values of the shear moduli (not exceeding 50 Pa), as well as their continuous thinning behavior during steady shear experiments.[25] Normally glasses have higher moduli by several orders of magnitude.[26−28] This is an important point as both gelation and glass transition are kinetic processes driven by crowding of the stars, which is induced by concentration and temperature. However, the gels and glasses (with interaction potential $U > 0$) relate to different length scales, larger (clusters) for the former and much smaller ("single particles" or segment length) for the latter.[29]

On the basis of unambiguous evidence such as that presented above, the following mechanism of the reversible thermal gelation is proposed: as the temperature increases, the solvent quality improves (Figure 2), and the peripheral blobs of the interacting liquid-ordered soft spheres swell; consequently, assuming overall incompressibility of the system, the spheres increase their arms' overlap, but not to a large extent because of the strong excluded-volume repulsions. This crowding eventually leads to a dynamic frustration (jamming) of the stars due to the formation of clusters consisting of a few "trapped" spheres, in equilibrium with "free" spheres.

The presence of clusters is supported by dynamic light scattering experiments[6] (probing a slow "cluster" mode at high temperatures, which disappears upon cooling; see also Figure 8) and pulsed-field gradient NMR measurements[6] (which probed the presence of two populations in the gelled stars). In addition, from the moduli in the "solid" regime (see for example Figures 4−7), the extracted typical average size $\xi = (kT/G')^{1/3}$ is slightly above the single R_h, conforming to the presence of some larger entities.The cartoon of Chart 2

attempts at representing a snapshot of this situation with the hypothetical bold periphery circumscribing an area of dynamic arrest (cluster). Note that a very low degree of clustering apparently suffices for the macroscopic immobilization of the system.[30] It is emphasized that swelling alone is not sufficient to provide appropriate conditions for heating-induced gelation; a high density of highly branched spherical brushes is needed for jamming to occur. In connection with this, even when swelling of grafted colloids (with rather low grafting density) upon heating was detected, a solidlike behavior was not observed.[31] On the other hand, in an athermal solvent gelation takes place by increasing volume fraction at high concentrations.[8] In that situation, strong gels relate to nonergodic behavior in light scattering and have higher moduli.[25] It is conceivable that the two gelation mechanisms (temperature-induced at constant concentration in this work vs concentration-induced at constant temperature in good solvents[8]) may be different; such a difference was recently observed for physical gels of poly(vinyl alcohol) and discussed in the context of site-bond percolation theory.[32]

It appears, therefore, that the star chain expansion upon heating is responsible for the slow formation of long-lived clusters (involving some kind of cooperativity) which kinetically arrest the system and form a gel, much like a glass formation process. Thus, the approach followed in this work provides solid evidence of a rather generic behavior for this class of soft materials, for which the size ratio of "grafted" layer to central core is about 100 times larger than in "conventional" micelles or sterically stabilized colloids used so far.[33] In addition, the present findings demonstrate how the effective volume fraction of these crowded soft systems can increase with temperature apart from density, offering a new route to reversible gelation. This is schematically shown in the inset of Figure 10, which illustrates the generalized jamming phase diagram proposed by Liu and Nagel,[1] which attempts to unify the different ways in which the ability of a soft system to flow can be lost. In the temperature-inverse density part of this diagram we added the alternative kinetic freezing possibilities suggested from the thermal gelation study of this work (liquid−gel boundary). Finally, this investigation represents another manifestation of the dramatic impact of weak external fields in inducing large macroscopic changes in this class of materials.[34,35]

IV. Concluding Remarks

We demonstrated that solutions of star polymers above the overlap concentration undergo a reversible thermal gelation. Using a combination of rheological and scattering techniques, this phenomenon was attributed to the formation of clusters causing a partial dynamic arrest of the swollen interpenetrating spheres at high temperatures. A jamming phase diagram of the gelation temeperature vs the effective volume fraction was shown to represent this gelation process, bringing analogies to glass formation. A small internal structural difference between regular and irregular stars, which did not influence their overall spherical shape, showed the large sensitivity of this phenomenon to molecular features, as it had a significant impact on the gelation temperature, yielding different gelation boundaries for regular ($f = 128$) and irregular ($f = 270$) stars. The obtained generalized kinetic pseudo-phase diagram is proposed as an alternative route to jamming.

Acknowledgment. J.R. acknowledges the hospitality of FO.R.T.H.-IESL in Heraklion. We are grateful to M. Kapnistos for his assistance with some of the measurements and to T. Pakula for helpful discussions. Partial support from the EU (Grant HPRN-CT-2000-00017) and the Greek Ministry of Education (Grant 1090-Applied Molecular Spectroscopy) is gratefully acknowledged.

References and Notes

(1) Liu, A. J.; Nagel, S. R. *Nature* **1998**, *21*, 396.
(2) Cates, M. E.; et al. *Phys. Rev. Lett.* **1998**, *81*, 1841. Cates, M. E. In *Soft and Fragile Matter. Nonequilibrium dynamics, metastability and flow*; Cates, M. E., Evans, M. R., Eds.; Institute of Physics Publishing: Bristol, 2000.
(3) Guenet, J. M. In *Molecular Interactions and Time-Space Organization in Macromolecular Systems;* Morishima, Y., et al., Eds.; Springer-Verlag: Berlin, 1999. Berghmans, M.; et al. *Macromolecules* **1994**, *27*, 7669.
(4) Pople, J. A.; et al. *Macromolecules* **1997**, *30*, 5721. Siqueira, D. F.; et al. *Macromolecules* **1994**, *27*, 234. Mortensen, K. *Europhys. Lett.* **1992**, *19*, 599.
(5) Roovers, J.; et al. *Macromolecules* **1993**, *26*, 4324. Grest, G. S.; et al. *Adv. Chem. Phys.* **1996**, *XCIV*, 67.
(6) Kapnistos, M.; et al. *Phys. Rev. Lett.* **2000**, *85*, 4072.
(7) Daoud, M.; Cotton, J. P. *J. Phys. (Paris)* **1982**, *43*, 531. Foerster, S.; et al. *Phys. Rev. Lett.* **1996**, *77*, 95.
(8) Roovers, J. *Macromolecules* **1994**, *27*, 5359.
(9) Witten, T. A.; et al. *Europhys. Lett.* **1986**, *2*, 137. Richter, D.; et al. *J. Phys. IV* **1993**, *C8*, 3. Willner, L.; et al. *Macromolecules* **1994**, *27*, 3821. Roovers, J.; Toporowski, P. M.; Douglas, J. *Macromolecules* **1995**, *28*, 7064.
(10) Likos, C. N.; et al. *Phys. Rev. Lett.* **1998**, *80*, 4450.
(11) Seghrouchni, R.; et al. *Europhys. Lett.* **1998**, *42*, 271. Semenov, A. N.; et al. *Langmuir* **1999**, *15*, 358.
(12) Fleischer, G.; et al. *Physica A* **2000**, *280*, 266. Watzlawek, M.; et al. *Phys. Rev. Lett.* **1999**, *82*, 5289.
(13) Roovers, J.; et al. *Macromolecules* **1989**, *22*, 1897.
(14) Likos, C. N.; et al. *Phys. Rev. E* **1998**, *58*, 6299.
(15) Dozier, W. D.; et al. *Macromolecules* **1991**, *24*, 2810.
(16) Marques, C. M.; et al. *Eur. Phys. J. B* **1998**, *3*, 353.
(17) Stiakakis, E.; Sigel, R.; Meier, G.; Vlassopoulos, D.; Fytas, G.; Roovers, J., unpublished data. Note that the 12880/*d*-tetradecane data were taken at KWS II, F2-Jülich, using neutron wavelength of 6 Å and three detector distances (2, 8, and 20 m).
(18) Loppinet, B.; Sigel, R.; Larsen, A.; Fytas, G.; Vlassopoulos, D.; Liu, G. *Langmuir* **2000**, *16*, 6480.
(19) Douglas, J. F.; Roovers, J.; Freed, K. F. *Macromolecules* **1990**, *23*, 4168.
(20) Foerster, S.; Zisenis, M.; Wenz, E.; Antonietti, M. *J. Chem. Phys.* **1996**, *104*, 9956.
(21) Winter, H. H.; Mours, M. *Adv. Polym. Sci.* **1997**, *134*, 165.
(22) Sato, T.; et al. *Macromolecules* **2000**, *33*, 1686.
(23) Bates, F. S.; Wiltzius, P. *J. Chem. Phys.* **1989**, *91*, 3258.
(24) Kapnistos, M.; et al. *Europhys. Lett.* **1996**, *34*, 513.
(25) Stiakakis, E.; et al., manuscript in preparation.
(26) Kob, W. In *Soft and Fragile Matter. Nonequilibrium dynamics, metastability and flow*; Cates, M. E., Evans, M. R., Eds.; Institute of Physics Publishing: Bristol, 2000.
(27) Bouchaud, J. P. In *Soft and Fragile Matter. Nonequilibrium dynamics, metastability and flow*; Cates, M. E., Evans, M. R., Eds.; Institute of Physics Publishing: Bristol, 2000. Cloitre, M.; et al. *Phys. Rev. Lett.* **2000**, *85*, 4819.
(28) van Megen, W.; Underwood, S. M. *Phys. Rev. Lett.* **1993**, *70*, 2766. Pusey, P. N. In *Liquids, Freezing and Glass Transition*; Hansen, J. P., Levesque, D., Zinn-Justin, J., Eds.; North-Holland: Amsterdam, 1991.
(29) Segrè, P. N.; et al. *Phys. Rev. Lett.* **2001**, *86*, 6042.
(30) Horst, R. H.; Winter, H. H. *Macromolecules* **2000**, *33*, 7538.
(31) Croucher, M. D.; Milkie, T. H. *Faraday Discuss. Chem. Soc.* **1983**, *76*, 261. Mewis, J.; et al. *AIChE J.* **1989**, *35*, 415.
(32) Shibayama, M.; et al. *Macromolecules* **2000**, *33*, 7868.
(33) Gast, A. P.; Russel, W. B. *Phys. Today* **1998**, *51*, 24. McDonnell, G. A.; Gast, A. P. *Phys. Rev. Lett.* **1997**, *30*, 435.
(34) Witten, T. A. *Rev. Mod. Phys.* **1999**, *71*, S367.
(35) Likos, C. N. *Phys. Rep.* **2001**, *348*, 267.

MA010788L